

Article

Separation and Recovery of Iron and Rare Earth from Bayan Obo Tailings by Magnetizing Roasting and $(\text{NH}_4)_2\text{SO}_4$ Activation Roasting

Yan Zhou ^{1,2}, He Yang ^{1,2,*}, Xiang-xin Xue ^{1,2} and Shuai Yuan ^{1,2}

¹ School of Metallurgy, Northeastern University, Shenyang 110819, China; yanzhouchn@gmail.com (Y.Z.); xuexx@mail.neu.edu.cn (X.X.); happyyuanshuai@163.com (S.Y.)

² Liaoning Key Laboratory of Recycling Science for Metallurgical Resources, Shenyang 110819, China

* Correspondence: yangh@smm.neu.edu.cn; Tel.: +86-130-024-36218

Academic Editors: Jae-chun Lee, Bong-Gyoo Cho and Kyoungkeun Yoo

Received: 27 April 2017; Accepted: 24 May 2017; Published: 27 May 2017

Abstract: A novel approach for recovery of iron and rare earth elements (REEs) from Bayan Obo tailings of Baotou, China, was developed by combining magnetizing roasting, magnetic separation, $(\text{NH}_4)_2\text{SO}_4$ activation roasting, and water leaching. Thermodynamic analysis of carbothermal reduction was conducted to determine the temperature of magnetizing roasting, and it agreed well with the experimental results. The maximum recovery of Fe reached 77.8% at 600 °C, and the grade of total Fe in the magnetic concentrate was 56.3 wt. %. An innovative approach, using water to leach REEs after $(\text{NH}_4)_2\text{SO}_4$ activation roasting, was used to extract REEs from magnetic separation tailings. The main influence factors of the leaching recovery during $(\text{NH}_4)_2\text{SO}_4$ activation roasting, were investigated with the mass ratio of $(\text{NH}_4)_2\text{SO}_4$ to magnetic separation tailings, roasting temperature and roasting time. The leaching recoveries of La, Ce and Nd reached 83.12%, 76.64% and 77.35%, respectively, under the optimized conditions: a mass ratio of 6:1, a roasting temperature of 400 °C and a roasting time of 80 min. Furthermore, the phase composition and reaction process during the $(\text{NH}_4)_2\text{SO}_4$ activation roasting were analyzed with X-ray diffraction (XRD), energy dispersive X-ray spectroscopy & scanning electron microscopy (EDS-SEM) and thermogravimetry & differential scanning calorimetry (TG-DSC), and the leaching solution and leaching residue were also characterized.

Keywords: magnetizing roasting; magnetic separation; rare earth; ammonium sulfate; roasting; leaching

1. Introduction

The Bayan Obo ore deposit located in Inner Mongolia of China is one of the world's largest iron-rare earth mines, the symbiosis of rare earth elements (REEs), iron, niobium, thorium scandium, fluorine, phosphorus, and other 71 elements [1]. The rare earth minerals are mainly comprised of bastnaesite (RECO_3F) and monazite (REPO_4). Since 1927, the Bayan Obo mine has been mined mainly for iron ore. A large amount of REEs, niobium, scandium, thorium, and other metal elements have been mined along with iron ore mining. Although in recent decades, the recovery of REE has been performed by low intensity magnetic separation, and high intensity magnetic separation and flotation, the utilization rate of mined REEs is only 10–15% [2]. Most rare earth ore are stockpiled in a tailings dam as a secondary resource [1,3]. By 2005, more than 150 million tons of the thorium-radioactive rare earth tailings, 90–95% of which were ground to $<76 \mu\text{m}$ [4,5], were stored at the tailings dam, with an area of 11 to 12 km^2 near to the Yellow River, not only causing environmental pollution, but also increasing the risk of dam breakage [6,7]. The average REEs grade of the tailing has been increased

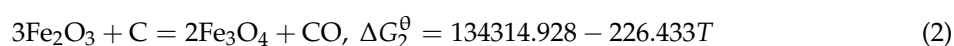
from 6.8% to 8.85%, which is almost close to, or even slightly higher than the grade of raw ore, due to the low recovery of REEs [7]. Recycling of such a large amount of rare earth resources is beneficial to environmental improvement, and is worth considerable economic value.

Currently, alkali treatment and acid treatment are commonly used for REEs recovery from high-grade rare earth concentrates; however, for low-grade ore, the two treatments are not economical [8,9]. In contrast, $(\text{NH}_4)_2\text{SO}_4$ activation roasting, a method used to recover valuable metals [10,11], can extract metallic elements from low-grade ore efficiently. In the process of $(\text{NH}_4)_2\text{SO}_4$ activation roasting, the ore was roasted with $(\text{NH}_4)_2\text{SO}_4$ at 200–600 °C. After roasting, valuable metals (such as La, Ce, Nd and etc.) were converted into corresponding sulfates, which are highly soluble in water. This method can be applied to extract metallic elements from Bayan Obo tailings, and deserves further investigation.

In this work, REEs were extracted from the Bayan Obo tailings by a combined process of magnetizing roasting, magnetic separation, $(\text{NH}_4)_2\text{SO}_4$ activation roasting, and water leaching. The Baiyun Obo tailings were sampled from low-intensity magnetic separation tailings. The magnetite (Fe_3O_4) in the raw ore was separated during the low intensity magnetic separation process, thus the REEs grade of the tailings were slightly higher than the raw ore. Magnetizing roasting and magnetic separation processes were then conducted to remove the hematite (Fe_2O_3) remaining in the Bayan Obo tailings [12]. It is notable that the RECO_3F and REPO_4 in the Bayan Obo tailings were decomposed into rare earth oxides during the process of magnetizing roasting, which was beneficial for further leaching recovery of REEs. The dissolution of rare earth oxides was significantly strengthened in the process of $(\text{NH}_4)_2\text{SO}_4$ activation roasting—La, Ce, Nd and other metallic element were converted into corresponding sulfates [13]. It was easy to obtain the rare earth sulfate solution by leaching using hot water. The main influencing factors on the leaching recovery of REEs, such as amount of $(\text{NH}_4)_2\text{SO}_4$, roasting temperature and roasting time, were investigated. Furthermore, the phase compositions of the Bayan Obo tailings before and after magnetizing roasting, of the leaching residue and the leaching solution were characterized; the phases and reactions during the $(\text{NH}_4)_2\text{SO}_4$ activation roasting process were analyzed. It was hoped that a novel technological process and theoretical basis for recycling REEs and iron from the Bayan Obo tailings could be developed.

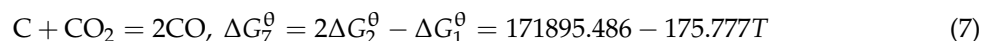
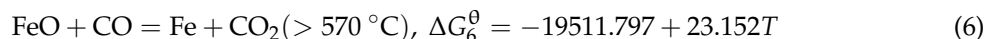
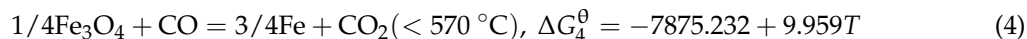
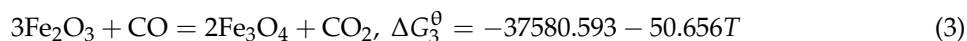
2. Thermodynamic Analysis of Carbothermic Reduction

Figure 1 shows the relationship between the temperature and Gibbs free energy of formation of Fe_2O_3 , Fe_3O_4 , FeO , CO , and CO_2 under standard conditions, which were calculated by the thermodynamic software FactSage version 7.0 (Thermfact/CRCT, Montreal, QC, Canada, 2015; GTT-Technologies, Aachen, Germany, 2015). The two intersections of the oxidation reaction line of Fe_3O_4 with the two lines of C indicated that Fe_2O_3 could be theoretically reduced to Fe_3O_4 by C when the temperature was above ~72 or ~322 °C, respectively. The reduction reactions of Fe_2O_3 are represented by Equations (1) and (2). The oxidation reaction lines of FeO , Fe and C intersect at temperatures in the range of 600–800 °C, indicating that FeO and Fe_3O_4 can be reduced by C, only when temperature is above ~600 °C. Therefore, it is feasible to reduce hematite (Fe_2O_3) to magnetite (Fe_3O_4) with coal (C), by controlling the temperature according to the thermodynamics of the reactions.



With the generation of CO in the Equation (2) reaction, Fe_2O_3 can be reduced to Fe by CO following a stepwise process, as shown in Equations (3)–(6). Since the activities of Fe_2O_3 , Fe_3O_4 , FeO and Fe (which are solid) are 1, the reaction equilibrium of Equations (3)–(6) can be represented as Equation (8). At normal pressure (1 atm), the state to which Fe_2O_3 will be reduced (Fe_3O_4 , FeO , or Fe), depends on the partial pressure of CO and CO_2 . The partial pressure of CO and CO_2 is determined by the gasification reaction of carbon (the Boudouard reaction) shown as Equation (7), which can be

calculated by the reaction of Equations (1) and (2). The reaction equilibrium of Equation (7) can also be represented as Equation (9).



$$\Delta G_i = \Delta G_i^\theta + RT \ln \frac{P_{\text{CO}}/P^\theta}{P_{\text{CO}_2}/P^\theta} \quad (8)$$

$$\Delta G_i = \Delta G_i^\theta + RT \ln \frac{(P_{\text{CO}}/P^\theta)^2}{a_{\text{C}} \times (P_{\text{CO}_2}/P^\theta)} \quad (9)$$

where ΔG_i is the actual Gibbs free energy change of Equations (3)–(7); ΔG_i^θ is the standard Gibbs free energy change of Equations (3)–(7); T is the temperature; a_i is the activity of the component i ; P_{CO} is the partial pressure of CO; P^θ is the normal pressure; and R is the universal gas constant. At normal pressure (1 atm), P_{CO} and P_{CO_2} have a relationship as shown in Equation (10).

$$P_{\text{CO}} + P_{\text{CO}_2} = P^\theta \quad (10)$$

According to the calculations of Equations (3)–(10), the equilibrium diagram of reduction of iron oxides by CO is represented in Figure 2.

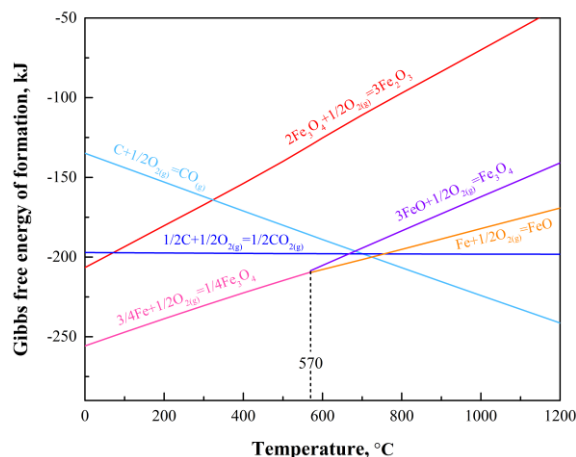


Figure 1. Relationship between temperature and Gibbs free energy of formation of oxides.

The reaction curve of Equation (3) in Figure 2 is very close to the horizontal axis; in other words, only a very low CO concentration can reduce Fe_2O_3 to Fe_3O_4 , so that this reaction is actually irreversible [14]. Figure 2 shows that CO concentration control is important. At normal pressure (1 atm), when the reaction of Equation (7) reaches equilibrium, P_{CO} in the system varies along the reaction curve of Equation (7) as temperature increases. When the temperature exceeds $\sim 650^\circ\text{C}$, the curve enters the stable area of FeO, which means that Fe_3O_4 will be reduced to FeO. Therefore, to avoid the reduction of Fe_3O_4 , the temperature should not exceed 650°C . Since the gas-solid reaction rate is greater than the solid-solid reaction rate, it is possible to increase the reduction efficiency by using the generated CO as a reductive agent at a suitable temperature.

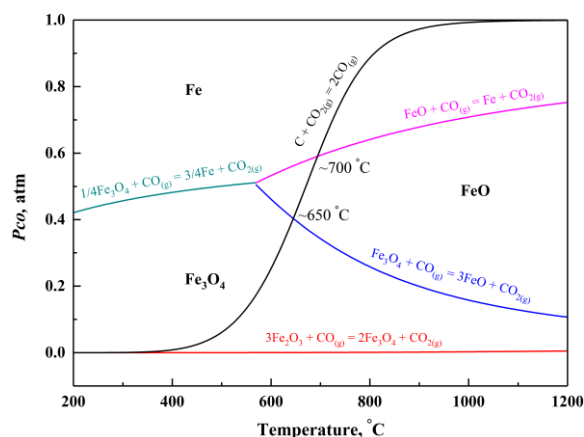


Figure 2. Equilibrium diagram of the reduction of iron oxides by CO.

Figure 3 shows the Fe–C–O predominance area diagram at 600 °C (873 K), calculated using the thermodynamic software FactSage version 7.0 [15], where the line made by “+” represents normal pressure (1 atm). The reduction of iron oxides by CO mainly depends on the partial pressure of CO and CO₂, which is consistent with the analysis above. Under normal pressure, Fe₃O₄ could exist when the partial pressure of CO is <~0.422 atm. It is deduced that the selection of the magnetizing roasting temperature as 600 °C, is appropriate.

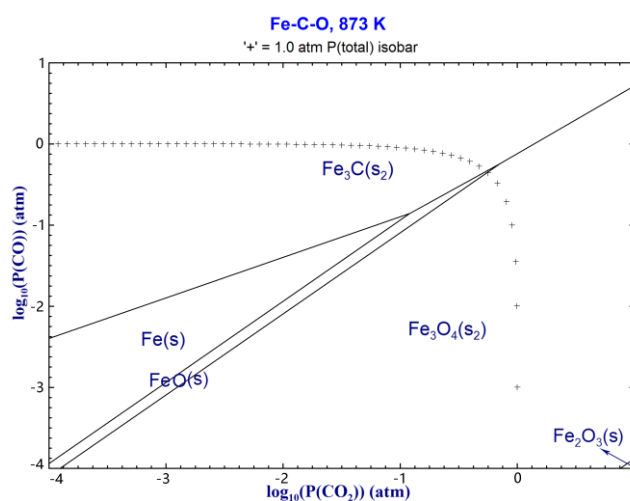


Figure 3. Predominance area diagram of Fe–C–O system at 600 °C (873 K).

3. Experimental Procedures

3.1. Magnetizing Roasting and Magnetic Separation

The Bayan Obo tailings used in this study were supplied by the Ore-Dressing Plant, Baotou Steel (Group) Co. (Baotou, China). The chemical compositions of the tailing samples shown in Table 1 were analyzed by X-ray Fluorescence Spectrometer (XRF) (model: ZSX Primus II, Rigaku Corporation, Tokyo, Japan) and chemical analysis. XRF was used to identify the elements in the tailings. Thereafter, the contents of each element were measured using chemical analysis according to Chinese standards (such as GB/T 17417.1–2010 for rare earth metals). The particle size distribution of the tailings was analyzed by a laser particle size analyzer (model: BT9300H, Dandong Bettersize Instruments Ltd., Dandong, China), shown in Table 2. Industrial pulverized coal was used as reducing agent; its chemical composition is shown in Table 3.

Table 1. Chemical composition of the sample of Bayan Obo tailings (wt. %).

Fe _{total}	FeO	REO	Nb ₂ O ₅	CaO	SiO ₂	BaO	MgO
13.06	2.10	7.09	0.103	30.34	11.71	4.13	3.32
Al ₂ O ₃	MnO	TiO ₂	F	S	P	Na ₂ O	K ₂ O
1.39	1.15	0.64	12.50	1.66	1.39	1.03	0.52

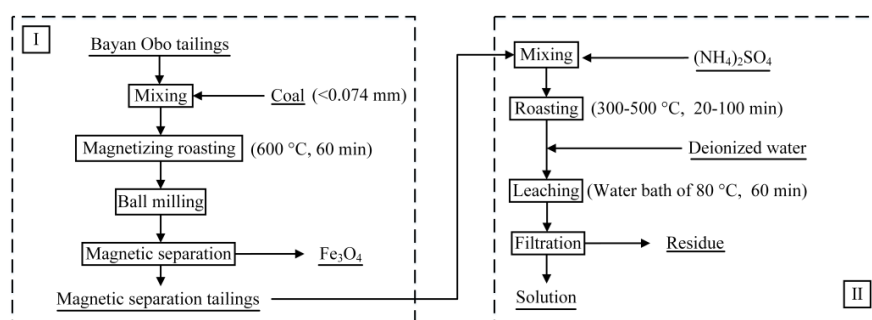
Table 2. Particle size distribution of the sample of Bayan Obo tailings (wt. %).

>149 μm	74–149 μm	58–74 μm	38–58 μm	<38 μm
9.29	25.05	30.71	32.10	2.85

Table 3. Chemical composition of the industrial pulverized coal (wt. %).

C	Volatile	Ash	SiO ₂	Al ₂ O ₃	P	S
83.66	6.62	9.33	4.81	1.47	<0.1	0.2

The magnetizing roasting experiments were carried out with a muffle furnace (Shenyang Great Wall Industrial Furnace, Shenyang, China). The Bayan Obo tailings (20 g) and pulverized coal (0.8 g, <0.074 mm) were mixed and pressed into a cylinder with a size of 30 mm in diameter, 10–12 mm in height at a pressure of 40 MPa. The cylindrical sample was sealed in a capped graphite crucible (Shenyang Metallurgical Graphite Factory, Shenyang, China) and roasted at 600 °C for 60 min. The graphite crucible was then removed and cooled by water. The roasting products were ball-milled at a speed of 120 rpm for 30 min. After milling, the roasting products were separated from the milling balls by washing with water. To separate the reduced magnetite from the roasting products, magnetic separation was carried out in a magnetic separation tube (Davis tube). This is a glass tube placed obliquely between two C type electromagnets. A magnetic field with a flux density of 125 mT was generated as a current running through the electromagnet. The mixture of material and water was poured from the high end of the glass tube at a constant rate. With the rotating and reciprocating movement of the glass tube in magnetic field, the magnetic substance attached to the tube wall, and the nonmagnetic substance was washed out with water. After magnetic separation, all the products were dried using a drying oven (Gongyi Yuhua Instrument Limited Liability Company, Gongyi, China). The process flow of this experiment is shown in Area I of Figure 4. The magnetic substance was a magnetic separation concentrate (mainly Fe₃O₄), and the nonmagnetic substance was comprised of magnetic separation tailings. The total Fe content of the magnetic separation concentrate was determined by the potassium dichromate volumetric method, and the REEs content of the magnetic separation tailings was determined by inductively coupled plasma optical emission spectrometry (ICP-OES). The wavelengths for analysis of La, Ce and Nd by ICP-OES are 408.672, 413.764 and 406.109 nm, respectively.

**Figure 4.** The process flow of the experiments.

3.2. $(\text{NH}_4)_2\text{SO}_4$ Activation Roasting and Water Leaching

The $(\text{NH}_4)_2\text{SO}_4$ activation experiments were carried out in a muffle furnace. The magnetic separation tailings and $(\text{NH}_4)_2\text{SO}_4$ were mixed with a specific mass ratio and poured into a porcelain crucible for roasting. The roasting temperature was in the range of 300–550 °C, and roasting time varied from 20 to 100 min according to the thermogravimetric results of $(\text{NH}_4)_2\text{SO}_4$ and the literature [16–18]. After $(\text{NH}_4)_2\text{SO}_4$ activation roasting, all of the product and deionized water (at a liquid-solid ratio of 10 mL/g) were poured into a beaker heated by a hot water bath. The temperature of the water bath was 80 °C. Then, the mixture was stirred at a speed of 400 rpm for 1 h. The leaching solution was filtered and diluted with deionized water to 500 mL. The leaching residues were dried using a drying oven. The process flow of this experiment is shown as Area II in Figure 4. The REEs content of the solutions was determined by ICP-OES.

4. Results and Discussion

4.1. Phase Change in Magnetizing Roasting

The phase composition of the Bayan Obo tailings was complex, as shown by X-ray diffraction (XRD) (PANalytical B.V., Almelo, Netherlands) in Figure 5. The peaks of fluorite (CaF_2), Fe_2O_3 and RECO_3F are clearly discernible. However, REPO_4 and other phases were not distinct, due to the weak peaks and overlapping. Scanning electron microscopy (SEM) (Carl Zeiss AG, Jena, Germany) images of mineralogical phases in the tailings and the energy dispersive X-ray spectroscopy (EDS) results are shown in Figures 6 and 7, and Table 4, respectively. The bright phases (marked as “A”), inlaid on a CaF_2 particle (marked as “B”), were REPO_4 . Besides, some Fe_2O_3 (marked as “C”), RECO_3F (marked as “D”), and dolomite ($\text{CaMg}(\text{CO}_3)_2$, marked as “E”) were observed on a micron scale.

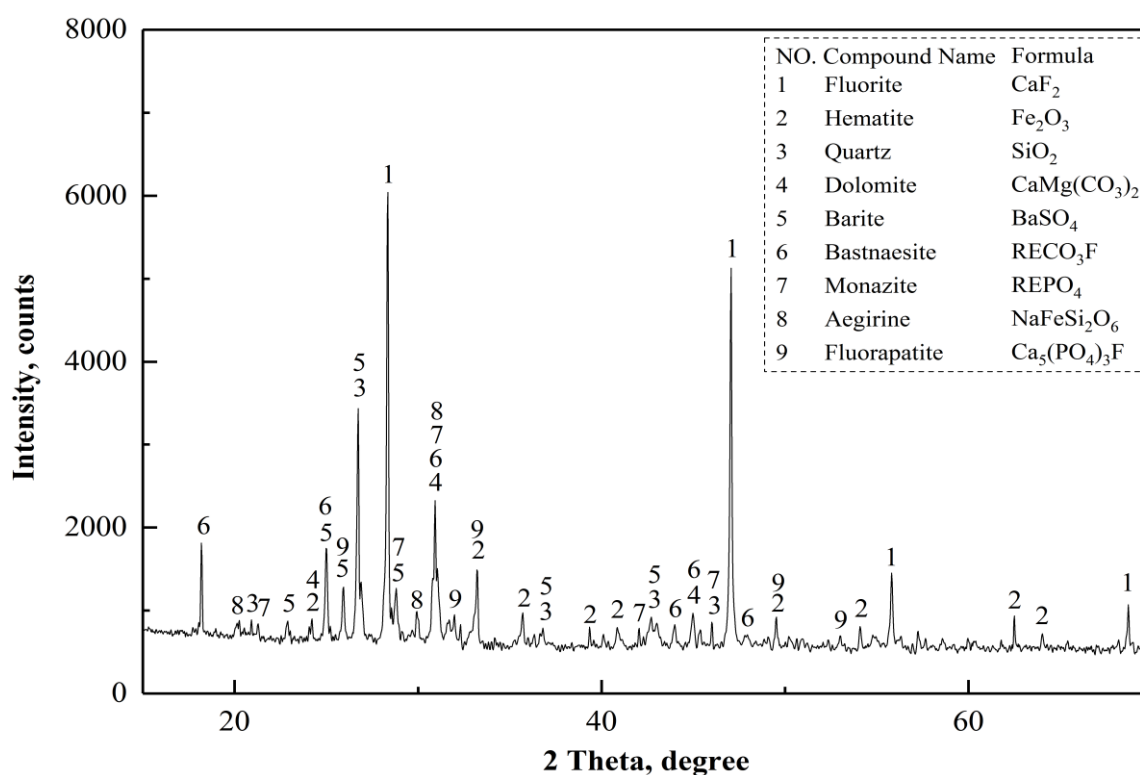


Figure 5. X-ray diffraction (XRD) patterns of Bayan Obo tailings.

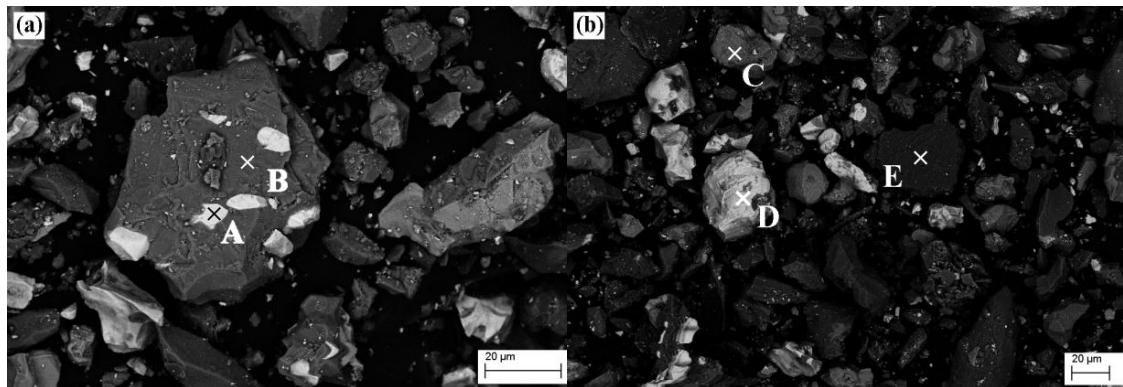


Figure 6. Scanning electron microscopy (SEM) images of the mineralogical phases in Bayan Obo tailings (a and b): (A) Monazite; (B) Fluorite; (C) Hematite; (D) Bastnaesite; (E) Dolomite.

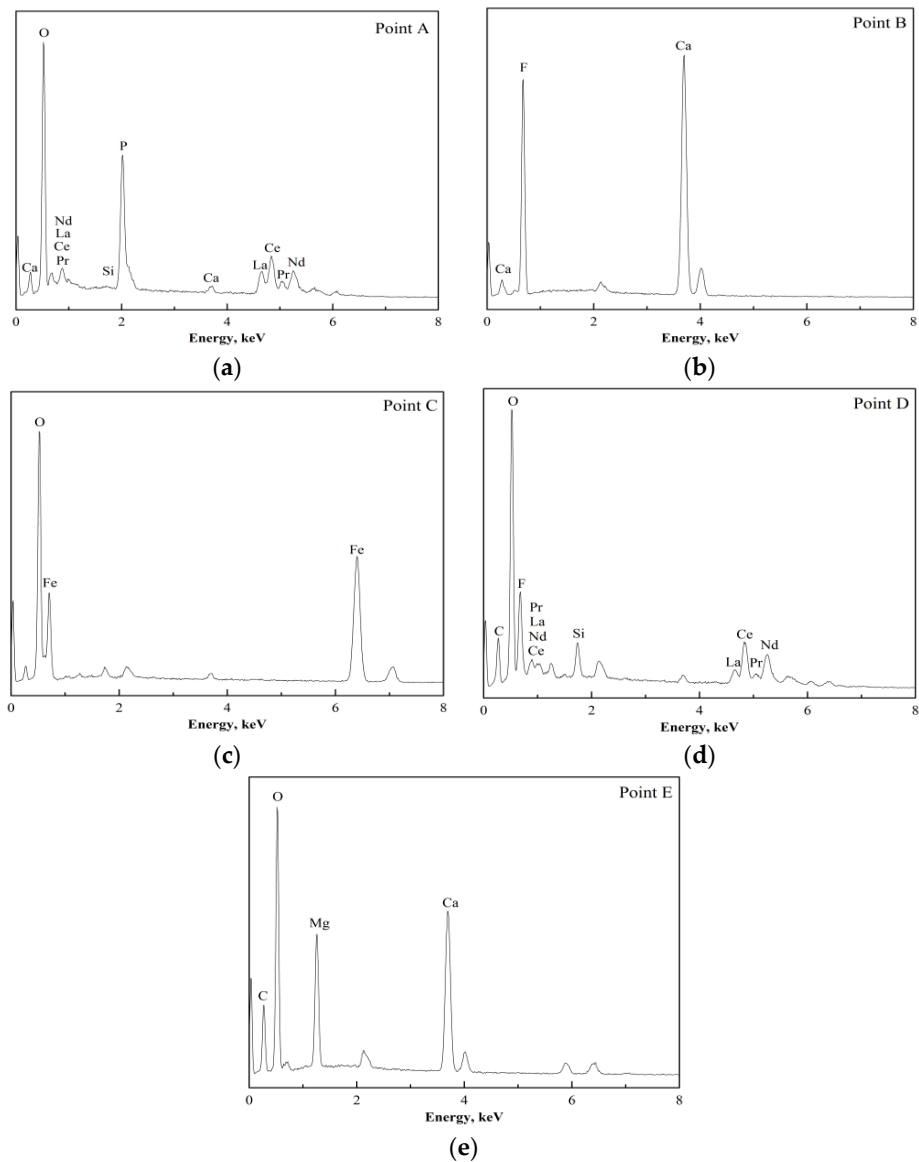
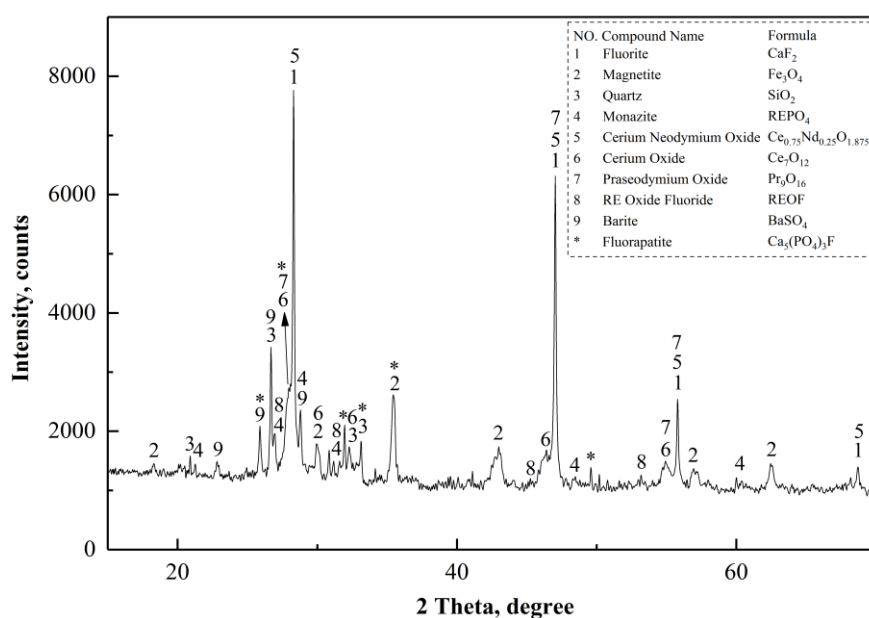


Figure 7. Energy dispersive X-ray spectroscopy (EDS) results for the mineralogical phases in Bayan Obo tailings: (a) Monazite; (b) Fluorite; (c) Hematite; (d) Bastnaesite; (e) Dolomite.

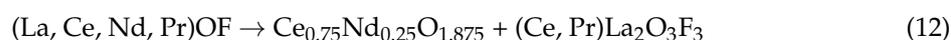
Table 4. Energy dispersive X-ray spectroscopy (EDS) results of the mineralogical phases in Bayan Obo tailings (wt. %).

Analysis Point	C	O	F	Mg	Si	P	Ca	Fe	La	Ce	Pr	Nd
A	-	27.61	-	-	-	13.42	1.12	-	16.84	30.04	3.26	7.70
B	-	-	51.09	-	-	-	48.91	-	-	-	-	-
C	-	29.75	-	-	-	-	-	70.25	-	-	-	-
D	9.16	25.02	8.39	1.21	2.77	-	1.01	2.33	8.80	28.90	2.82	9.58
E	53.49	-	-	11.30	-	-	28.19	7.02	-	-	-	-

Figure 8 shows the XRD pattern of the product after magnetizing roasting at 600 °C for 60 min, indicating that Fe₂O₃ was almost completely transformed to Fe₃O₄. The peaks of RECO₃F disappeared, and the peaks of REEs oxides (Ce_{0.75}Nd_{0.25}O_{1.875}, Ce₇O₁₂, Pr₉O₁₆, REOF) occurred, indicating that RECO₃F was decomposed at 600 °C; the peaks of some REEs oxides and CaF₂ overlapped with each other, showing strong intensity. REPO₄ was still observed, indicating that REPO₄ was more difficult to completely decompose at 600 °C.

**Figure 8.** XRD patterns of product after magnetizing roasting at 600 °C.

The corresponding SEM images are shown in Figure 9. The EDS results of the marked points in Figure 9 are shown in Figure 10 and Table 5. Comparing with bastnaesite particles before roasting (as marked as “D” in Figure 6), cracks occurred on the surface of roasted bastnaesite particles (marked as “F” in Figure 9). This could be attributed to the fact that CO₂ escapes from RECO₃F during decomposition. The decomposition theory could be expressed with Equations (11)–(13) [19]. Particles of Fe₃O₄ (Figure 9, marked as “G”) were cracked, this could be attributed to the change in volume caused by crystal structure changes when Fe₂O₃ were reduced to Fe₃O₄.



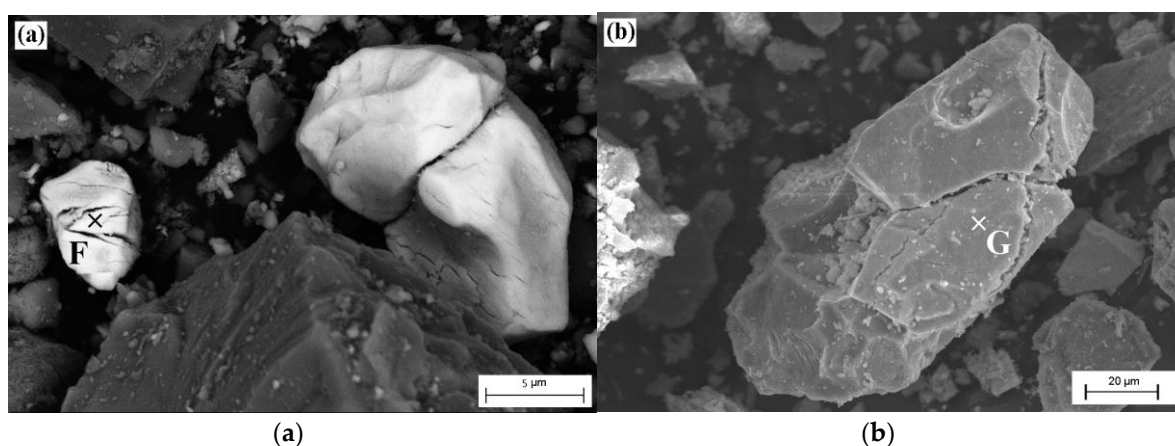


Figure 9. SEM images of mineralogical phases in Bayan Obo tailings after magnetizing roasting at 600 °C (a and b): (F) roasted bastnaesite; (G) Fe_3O_4 .

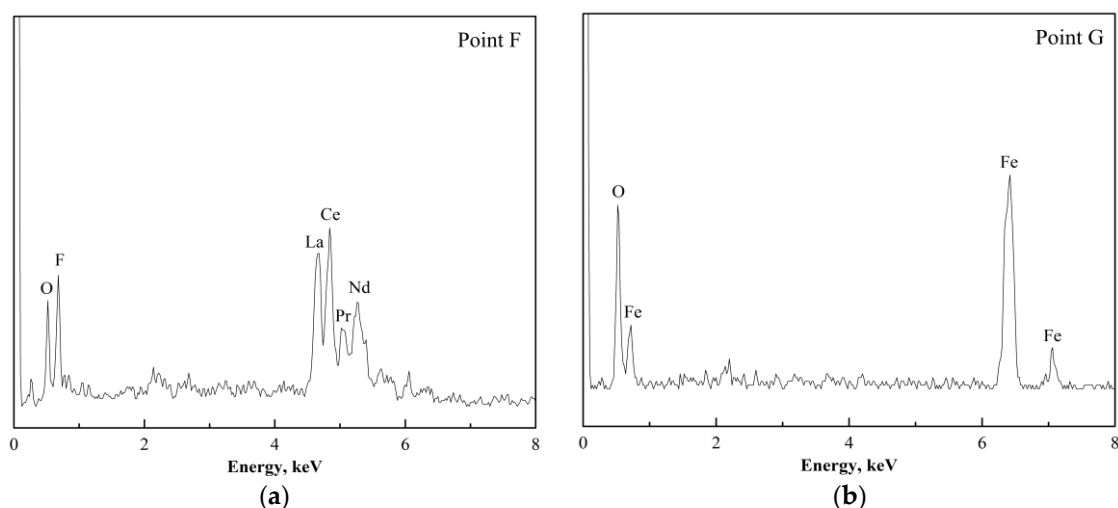


Figure 10. EDS results from Bayan Obo tailings after magnetizing roasting at 600 °C: (a) roasted bastnaesite; (b) Fe_3O_4 .

Table 5. EDS results from Bayan Obo tailings after magnetizing roasting at 600 °C. (wt. %).

Analysis Point	O	F	Fe	La	Ce	Pr	Nd
F	8.91	11.88	-	31.80	37.42	1.68	8.31
G	26.45	-	73.55	-	-	-	-

4.2. Behavior of Fe and Rare Earth Elements (REEs) in the Magnetic Separation Process

The grade and recovery of total Fe in the magnetic separation concentrate prepared at various magnetizing roasting temperatures are shown in Figure 11. The variation trends of grade with roasting temperature was consistent with the one of recovery: there was an initial increase with temperature, then a reduction after the temperature exceeded a specific value. At a relatively low temperature, the reduction efficiency of Fe_2O_3 was low, due to the low partial pressure of CO, resulting in low recovery and grade of total Fe. When the roasting temperature reached 600 °C, the grade and recovery of Fe in magnetic separation concentrate reached maximum, being 56.3 wt. % and 77.8%, respectively. Most of the Fe was recovered from the initial tailings through magnetizing roasting and magnetic separation. When the temperature exceeded 600 °C, the grade of total Fe decreased due to the Fe_3O_4 being further

reduced to FeO. The experimental results showed good agreement with the theoretical analysis in Section 2.

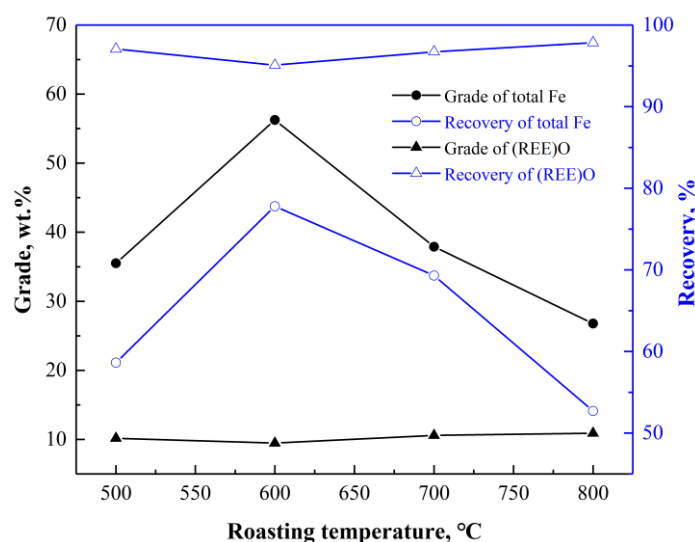


Figure 11. Grade and recovery of total Fe and (REE)O in the magnetic separation concentrate and tailings.

The grade and recovery of (REE)O in the magnetic separation tailings obtained at different magnetizing roasting temperatures are also shown in Figure 11. It was found that the recovery and grade of (REE)O did not change much with increasing temperature. After magnetic separation, the grade of (REE)O increased to approximately 10 wt. % from 7.09 wt. % for the initial tailing. More than 95% of REEs were recycled in all of the experiments, indicating that almost all the REE-bearing minerals were separated from magnetite (Fe_3O_4) by magnetic separation.

4.3. Phase Analysis and Reaction in $(\text{NH}_4)_2\text{SO}_4$ Activation Roasting

Figure 12 shows the results of thermogravimetry (TG) and differential scanning calorimetry (DSC) analysis results for $(\text{NH}_4)_2\text{SO}_4$. The analytical equipment used was the SDT 2960 Simultaneous DSC-TGA manufactured by TA Instruments (New Castle, Delaware, DE, USA). The TG–DSC curve of $(\text{NH}_4)_2\text{SO}_4$ indicated thermal decomposition between 200–500 °C, with the process expressed using Equations (14)–(19) [16–18]. Obviously, the thermal decomposition of $(\text{NH}_4)_2\text{SO}_4$ is a complex process. Thermal decomposition reactions can be divided into three steps [20,21], as shown in Table 6. The intermediate products during thermal decomposition, NH_4HSO_4 , $(\text{NH}_4)_3\text{H}(\text{SO}_4)_2$, $\text{NH}_2\text{SO}_3\text{H}$, and $(\text{NH}_4)_2\text{S}_2\text{O}_7$, are known as acidifying agents. These acidifying agents perform better under “acidification” than the aqueous solution of $(\text{NH}_4)_2\text{SO}_4$. Thus, rare earth oxides can be decomposed into rare earth ions by acidifying agents within the temperature range of 200–500 °C.

Figure 13 shows the TG–DSC curve of the mixture of the magnetic separation tailings and $(\text{NH}_4)_2\text{SO}_4$ in a mass ratio of 4:1. In contrast to the TG–DSC curve of $(\text{NH}_4)_2\text{SO}_4$ shown in Figure 12, the number of the endothermic peaks and the peak temperature of the endothermic peaks changed. The peak at 312 °C indicated the occurrence of thermal decomposition of $(\text{NH}_4)_2\text{SO}_4$ and the formation of $\text{NH}_4\text{RE}(\text{SO}_4)_2 \cdot 4\text{H}_2\text{O}$. The peak at 437 °C indicated the thermal decomposition of $\text{NH}_4\text{RE}(\text{SO}_4)_2 \cdot 4\text{H}_2\text{O}$ and residual acidifying agents.

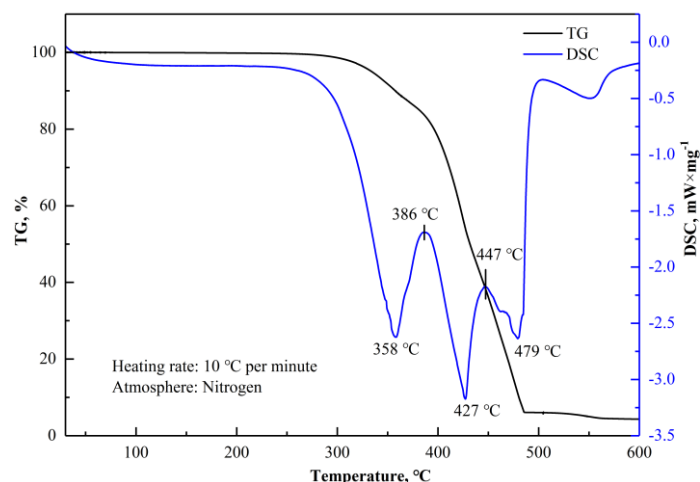


Figure 12. The thermogravimetry–differential scanning calorimetry (TG-DSC) curve of $(\text{NH}_4)_2\text{SO}_4$.

Table 6. Thermal decomposition reaction of $(\text{NH}_4)_2\text{SO}_4$.

Step	Temperature	Reaction
1	200–386 °C	$(\text{NH}_4)_2\text{SO}_4 \rightarrow \text{NH}_4\text{HSO}_4 + \text{NH}_3\uparrow$ (14)
		$2(\text{NH}_4)_2\text{SO}_4 \rightarrow (\text{NH}_4)_3\text{H}(\text{SO}_4)_2 + \text{NH}_3\uparrow$ (15)
		$\text{NH}_4\text{HSO}_4 \rightarrow \text{NH}_2\text{SO}_3\text{H} + \text{H}_2\text{O}\uparrow$ (16)
2	386–447 °C	$\text{NH}_4\text{HSO}_4 + \text{NH}_2\text{SO}_3\text{H} \rightarrow (\text{NH}_4)_2\text{S}_2\text{O}_7$ (17)
		$2\text{NH}_4\text{HSO}_4 \rightarrow (\text{NH}_4)_2\text{S}_2\text{O}_7 + \text{H}_2\text{O}\uparrow$ (18)
3	447–500 °C	$3(\text{NH}_4)_2\text{S}_2\text{O}_7 \rightarrow 2\text{NH}_3\uparrow + 2\text{N}_2\uparrow + 6\text{SO}_2\uparrow + 9\text{H}_2\text{O}\uparrow$ (19)

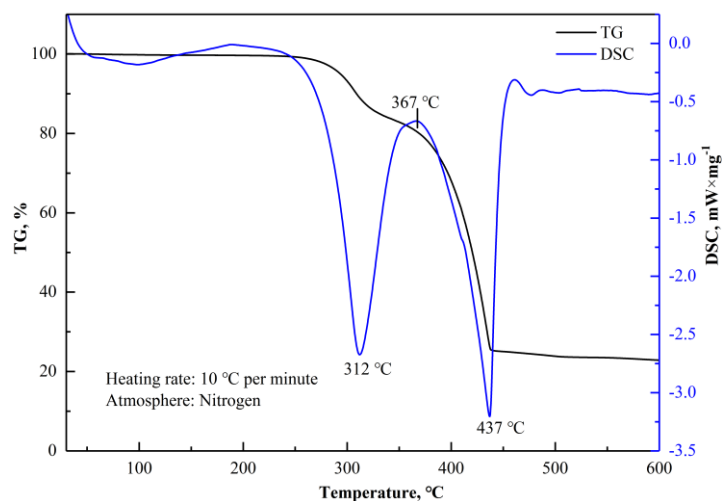


Figure 13. The TG-DSC curve of the mixture of magnetic separation tailings and $(\text{NH}_4)_2\text{SO}_4$ in mass ratio of 4:1.

Activation roasting experiments were conducted at various temperatures, and the products were analyzed by XRD, as shown in Figure 14.

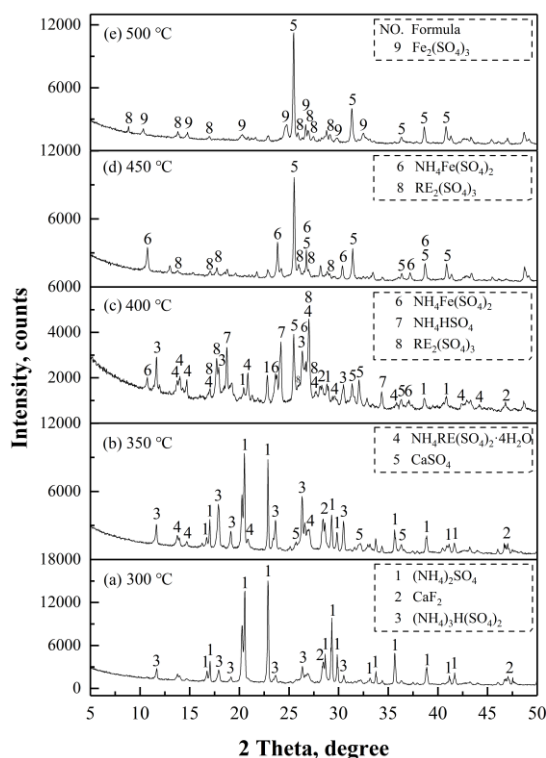
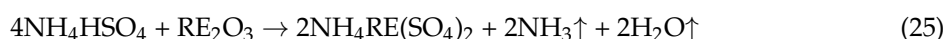
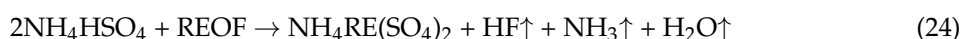
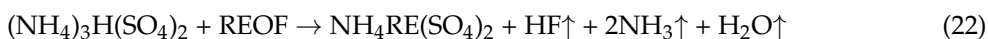
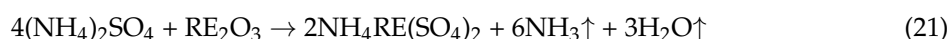
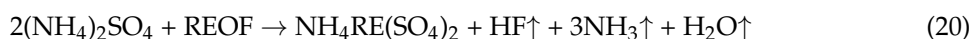
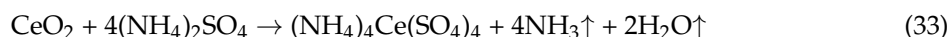
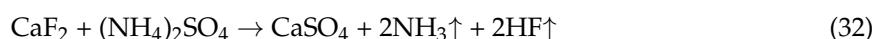
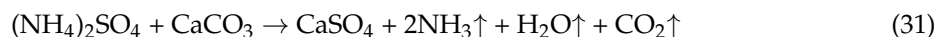
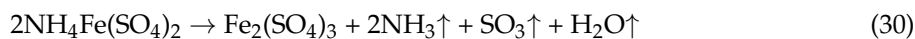
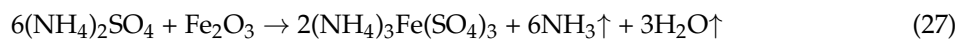
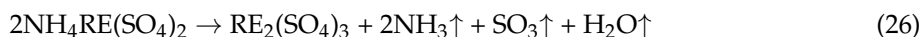


Figure 14. XRD patterns of $(\text{NH}_4)_2\text{SO}_4$ activation roasting products at different temperatures: (a) 300 °C; (b) 350 °C; (c) 400 °C; (d) 450 °C; (e) 500 °C.

$(\text{NH}_4)_3\text{H}(\text{SO}_4)_2$ was the only product observed in Figure 14a, indicating that the dominant reaction was Equation (15), when the roasting temperature reached 300 °C. As for the increase of temperature, the reactions of Equations (20)–(25), (31), and (32) occurred at 350 °C, corresponding to the first endothermic peak in Figure 13, with the products of CaSO_4 and $\text{NH}_4\text{RE}(\text{SO}_4)_2 \cdot 4\text{H}_2\text{O}$ as shown in Figure 14b. The formation of $\text{NH}_4\text{Fe}(\text{SO}_4)_2$, NH_4HSO_4 and $\text{RE}_2(\text{SO}_4)_3$ at 400 °C, shown in Figure 14c, implied that $\text{NH}_4\text{RE}(\text{SO}_4)_2 \cdot 4\text{H}_2\text{O}$ and $(\text{NH}_4)_2\text{SO}_4$ continued to decompose, and ferruginous minerals (residual Fe_2O_3 and Fe_3O_4 , $\text{NaFeSi}_2\text{O}_6$, FeS) reacted with the acidifying agents. The characteristic peaks of $(\text{NH}_4)_2\text{SO}_4$, NH_4HSO_4 and $\text{NH}_4\text{RE}(\text{SO}_4)_2 \cdot 4\text{H}_2\text{O}$ disappeared at 450 °C, as shown in Figure 14d, which were attributed to the complete decomposition of $\text{NH}_4\text{RE}(\text{SO}_4)_2 \cdot 4\text{H}_2\text{O}$, $(\text{NH}_4)_2\text{SO}_4$, and the residual acidifying agents, corresponding to the second endothermic peak in Figure 13. When the temperature reached 500 °C, $\text{NH}_4\text{Fe}(\text{SO}_4)_2$ completely decomposed into $\text{Fe}_2(\text{SO}_4)_3$, as shown in Figure 14e. The reactions between the magnetic separation tailings and $(\text{NH}_4)_2\text{SO}_4$ which may occur at roasting temperatures from 200 to 500 °C, are expressed with Equations (20)–(32). In addition, the reaction (Equation (33)) between CeO_2 and $(\text{NH}_4)_2\text{SO}_4$ at 250 °C was also included, which is confirmed by Mudher K.D.S et al. [13].





$\text{NH}_4\text{RE}(\text{SO}_4)_2 \cdot 4\text{H}_2\text{O}$ and $\text{RE}_2(\text{SO}_4)_3$ are soluble in water, providing a feasible way to extract REEs by water leaching. According to the above analysis and TG-DSC curves in Figures 12 and 13, the roasting temperature should be controlled below 400 °C to avoid rapid decomposition and mass loss of $(\text{NH}_4)_2\text{SO}_4$, which is detrimental to the formation of $\text{NH}_4\text{RE}(\text{SO}_4)_2 \cdot 4\text{H}_2\text{O}$.

The morphology of the products after $(\text{NH}_4)_2\text{SO}_4$ activation roasting at various temperatures was examined by SEM-EDS. Figure 15a shows the particles roasted at 400 °C. The particles were covered with sulfates ($\text{NH}_4\text{RE}(\text{SO}_4)_2 \cdot 4\text{H}_2\text{O}$, CaSO_4 , $(\text{NH}_4)_2\text{SO}_4$, etc.) as indicated by the letter I in Figure 15a. The white phase (marked as “H” in Figure 15a) on the surface of particles was identified as BaSO_4 .

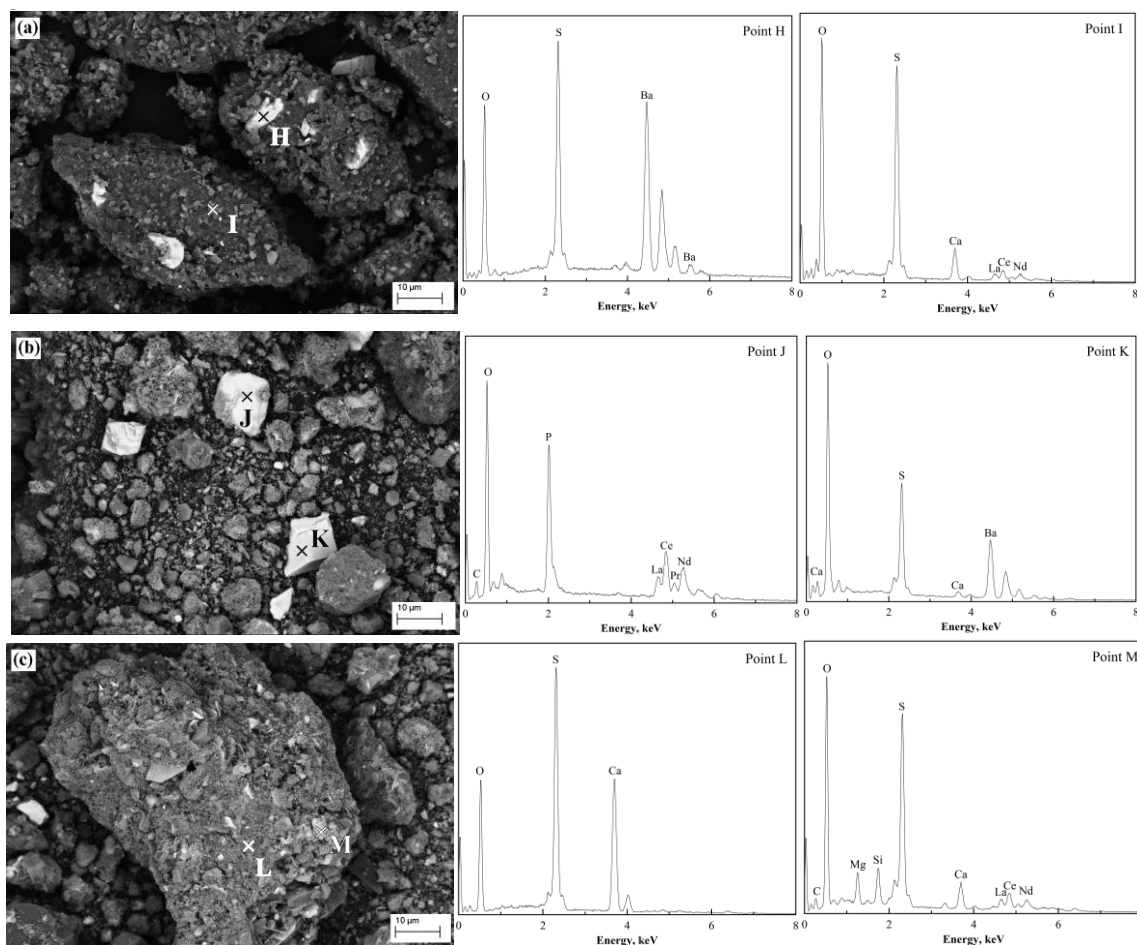


Figure 15. SEM image and EDS spectra of the $(\text{NH}_4)_2\text{SO}_4$ activation roasting products: (a) 400 °C; (b,c) 500 °C.

The micrograph of roasting products at 500 °C shows a non-uniform distribution in particle size, as shown in Figure 15b,c. The bright phases (marked as “J” and “K”) were REPO_4 and BaSO_4 respectively, indicating that they hardly reacted with $(\text{NH}_4)_2\text{SO}_4$ or the acidifying agents. The larger particle in Figure 15c consisted of CaSO_4 (marked as “L”) and other sulfates (marked as “M”) such as $\text{RE}_2(\text{SO}_4)_3$ and MgSO_4 . The morphology shown in Figure 15c was different from the one shown in Figure 15a, because there was no residual $(\text{NH}_4)_2\text{SO}_4$ on the surface, after roasting at 500 °C.

4.4. Effect of Temperature on the Leaching Recovery of REEs during $(\text{NH}_4)_2\text{SO}_4$ Activation Roasting

The leaching recovery of REEs was defined as the ratio of the mass of REEs in the leaching solution to the mass of REEs in the tailings before leaching. Water leaching tests were carried out with different samples produced via $(\text{NH}_4)_2\text{SO}_4$ activation roasting at different temperatures. The mass ratio of $(\text{NH}_4)_2\text{SO}_4$ to the tailings was 4:1, and the duration of the roasting process was 60 min. The trends of leaching recovery with the roasting temperature for La, Ce and Nd are shown in Figure 16. The leaching recoveries increased sharply in the temperature range of 300–400 °C, and reached a maximum at 400 °C. The maximum values for La, Ce and Nd were 78.75%, 75.57%, and 75.89%, respectively.

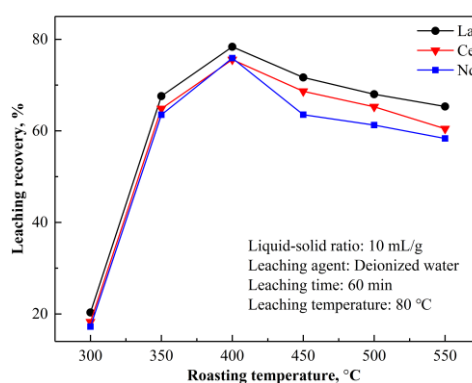


Figure 16. Effect of $(\text{NH}_4)_2\text{SO}_4$ activation roasting temperature on the leaching recoveries of La, Ce, and Nd.

According to the above analysis, $(\text{NH}_4)_2\text{SO}_4$ started to become liquefied and decomposed at 300 °C. Due to the lack of molten $(\text{NH}_4)_2\text{SO}_4$ and “acidifying agents”, the formation of $\text{NH}_4\text{RE}(\text{SO}_4)_2 \cdot 4\text{H}_2\text{O}$ was quite slow before 300 °C, resulting in low leaching recovery. With the rise of temperature, molten $(\text{NH}_4)_2\text{SO}_4$ and the acidifying agents increased, promoting the leaching recoveries of La, Ce and Nd by generating large amounts of $\text{NH}_4\text{RE}(\text{SO}_4)_2 \cdot 4\text{H}_2\text{O}$. However, after temperatures exceeding 400 °C, $(\text{NH}_4)_2\text{SO}_4$ and the acidifying agents started to decompose rapidly, verified by the TG–DSC results in Figure 12. The generation of $\text{NH}_4\text{RE}(\text{SO}_4)_2 \cdot 4\text{H}_2\text{O}$ was cut down due to the lack of molten $(\text{NH}_4)_2\text{SO}_4$ and acidifying agents, leading to a drop in leaching recovery. It was easily concluded that the optimum temperature for roasting should be 400 °C.

4.5. Effect of $(\text{NH}_4)_2\text{SO}_4$ Activation Roasting Time on the Leaching Recovery of REEs

Figure 17 shows the relationship of roasting time to the leaching recoveries of La, Ce and Nd by activation roasting, under identical conditions: a roasting temperature of 400 °C, and the mass ratio of $(\text{NH}_4)_2\text{SO}_4$ to magnetic separation tailings being 4:1.

Leaching recovery continued to increase as roasting time increased, and reached maximum after 80 min. The maximum leaching recoveries for La, Ce and Nd were 81.13%, 76.29% and 79.58%, respectively. Before 80 min, the roasting time was too short for $(\text{NH}_4)_2\text{SO}_4$ to become completely liquefied, resulting in insufficient generation of $\text{NH}_4\text{RE}(\text{SO}_4)_2 \cdot 4\text{H}_2\text{O}$ and $\text{RE}_2(\text{SO}_4)_3$. The acidity of the leaching solution was maintained with residual $(\text{NH}_4)_2\text{SO}_4$, preventing hydrolysis of $\text{RE}_2(\text{SO}_4)_3$ to form precipitates. When the roasting time exceeded 80 min, $(\text{NH}_4)_2\text{SO}_4$ were excessively consumed

and decomposed, resulting in a lack of residual $(\text{NH}_4)_2\text{SO}_4$. The two phenomena all led to the decrease of leaching recovery.

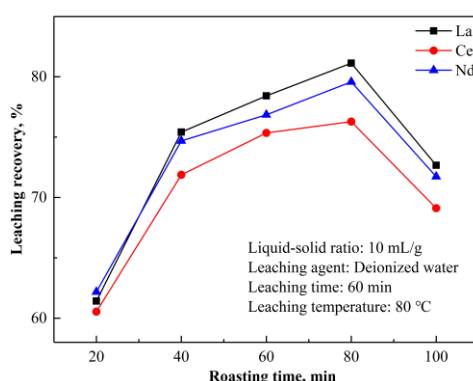


Figure 17. Effect of $(\text{NH}_4)_2\text{SO}_4$ activation roasting time on the leaching recoveries of La, Ce, and Nd.

4.6. Effect of the Mass Ratio on the Leaching Recovery of REEs

A series of experiments were conducted at $400\text{ }^\circ\text{C}$ for 80 min, to investigate the influence of the mass ratio of $(\text{NH}_4)_2\text{SO}_4$ on magnetic separation tailings for the leaching recoveries of La, Ce and Nd. The results are shown in Figure 18, showing that the leaching recoveries of La, Ce and Nd reached the maximum value of 83.12%, 76.64% and 77.35%, respectively, at a mass ratio of 6:1.

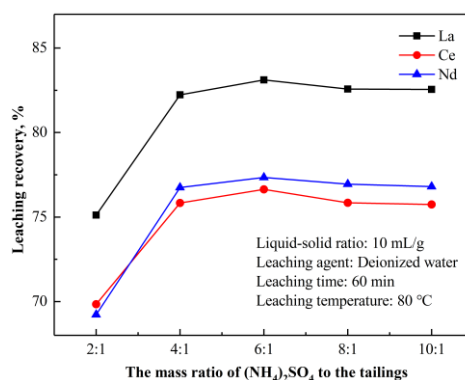


Figure 18. Effect of the mass ratio on the leaching recoveries of La, Ce, and Nd.

During the roasting process, the more the molten $(\text{NH}_4)_2\text{SO}_4$ and the acidifying agents were, the deeper the degree of reactivity (Equations (20)–(25)). Before reaching a ratio of 6:1, the increase in mass ratio led to an increase in leaching recovery. However, a further increase in $(\text{NH}_4)_2\text{SO}_4$ led to excessive NH_4^+ and SO_4^{2-} in the leaching solution. The REEs ions then tended to precipitate with extra NH_4^+ and SO_4^{2-} , in form of $\text{NH}_4\text{RE}(\text{SO}_4)_2$, leading to the loss of REEs.

4.7. Phase Analysis of the Leaching

The phase composition of leaching residues was analyzed by XRD and EDS. The results were shown in Figure 19 and Table 7. It showed that the leaching residues were mainly composed of CaF_2 , CaSO_4 , SiO_2 and BaSO_4 . The morphologies of the leaching residues were shown in Figures 20 and 21. The bright phases as shown in Figure 20a, were BaSO_4 (marked as “N”) and REPO_4 (marked as “O”), respectively; the dark phases were SiO_2 (marked as “P”). The rod-like phases (marked as “Q”) in Figure 20b were CaSO_4 , which were the new phases formed during the leaching process. The possible reason for the residual CaF_2 is that CaSO_4 was formed on the surface of CaF_2 particles during the

roasting process, preventing further reaction between $(\text{NH}_4)_2\text{SO}_4$ and CaF_2 . The REEs in the leaching residues were mainly found in undecomposed monazite (REPO_4), which is the reason why the leaching recovery of REEs was less than 90%.

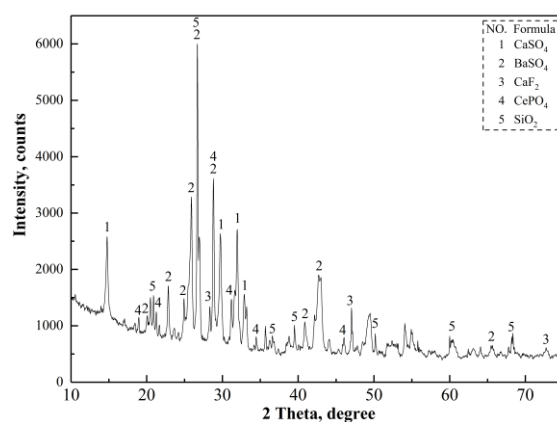


Figure 19. XRD patterns of the leaching residues.

Table 7. Chemical composition of the leaching residues (wt. %).

Fe	REO	CaO	SO_4^{2-}	CaF_2	SiO_2	BaO	P	MgO	Al_2O_3
1.10	3.74	4.60	13.86	29.09	15.62	6.27	1.03	0.68	0.57

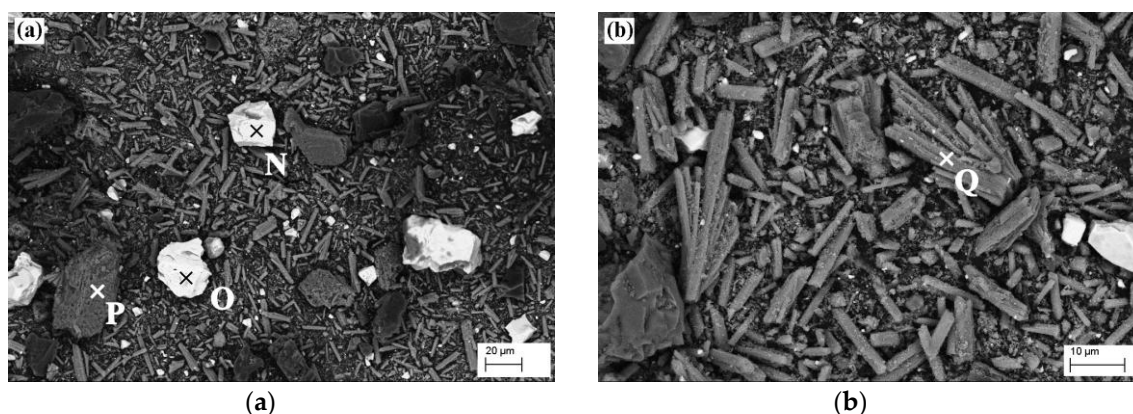


Figure 20. SEM image of the leaching residues (a and b): (N) BaSO_4 ; (O) REPO_4 ; (P) SiO_2 ; (Q) CaSO_4 .

Figure 22 shows the XRD pattern of the precipitated crystals obtained after drying the leaching solution, indicating that the main ion components in the leaching solution were NH_4^+ , SO_4^{2-} , HSO_4^- , Fe^{3+} , RE^{3+} and Ca^{2+} . The concentrations of La, Ce and Nd in the leaching solution were measured by ICP-OES, which were 0.407, 0.740 and 0.232 g/L, respectively, under the optimum conditions. The REEs elements could be precipitated by adjusting the pH of the leaching solution using the ammonia gas released from the $(\text{NH}_4)_2\text{SO}_4$ activation roasting process. The REEs precipitate was then dissolved in an acid solution, from which the REEs could be recycled by solvent extraction. The $(\text{NH}_4)_2\text{SO}_4$ in the solution could be recycled by concentrating the solution to precipitate the crystals.

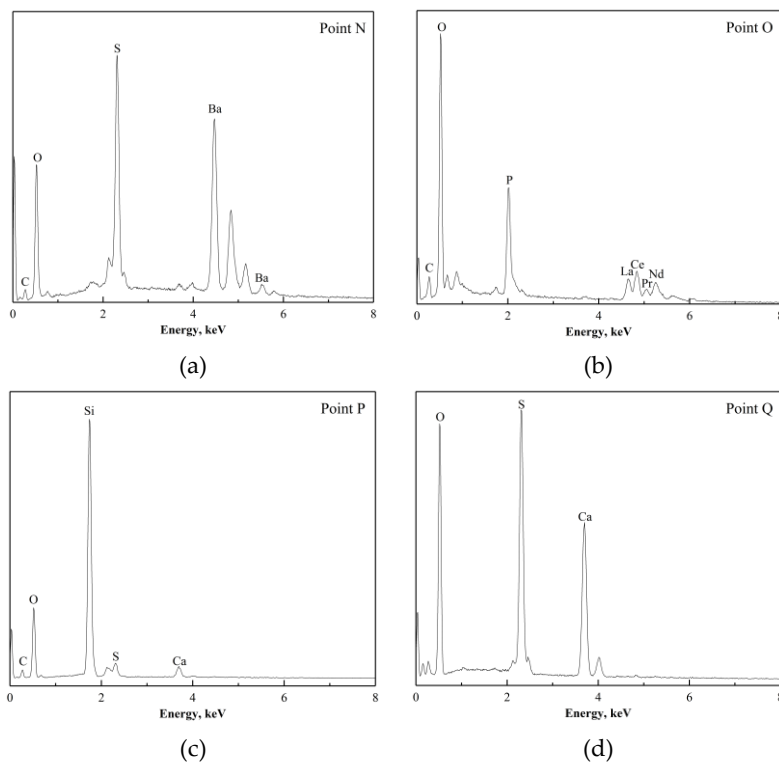


Figure 21. EDS spectra of the leaching residues: (a) BaSO_4 ; (b) REPO_4 ; (c) SiO_2 ; (d) CaSO_4 .

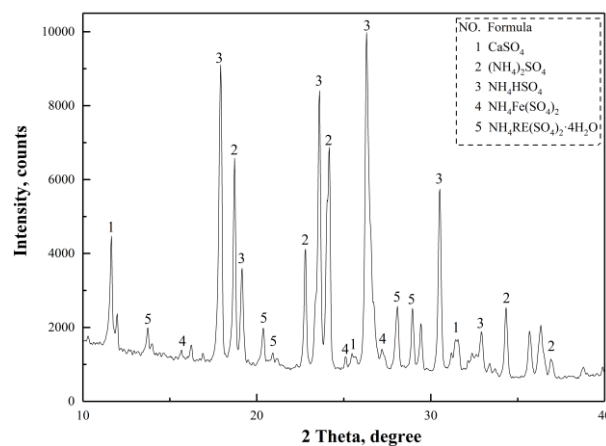


Figure 22. XRD pattern of the crystal precipitation.

5. Conclusions

In this study, a novel approach combining magnetizing roasting, magnetic separation, $(\text{NH}_4)_2\text{SO}_4$ activation roasting, and leaching using water was developed to extract REEs and iron from Bayan Obo tailings. The following are the principal conclusions drawn from the theoretical and experimental work:

(1) The magnetizing roasting temperature of $600\text{ }^\circ\text{C}$ was determined through thermodynamic analysis, agreeing well with the experimental results. The maximum recovery of Fe reached 77.8% at the temperature of $600\text{ }^\circ\text{C}$, and the grade of total Fe in the magnetic concentrate was 56.3 wt. %. Higher temperatures led to the reduction of Fe_3O_4 , and lower temperatures tended to lower the partial pressure of CO, both of which led to the loss of Fe during the magnetic separation.

(2) An innovative approach, using water to leach REEs after $(\text{NH}_4)_2\text{SO}_4$ activation roasting, was used to extract REEs from magnetic separation tailings. The main influencing factors of the leaching

recovery during $(\text{NH}_4)_2\text{SO}_4$ activation roasting, were investigated with the mass ratio of $(\text{NH}_4)_2\text{SO}_4$ to magnetic separation tailings, roasting temperature, and roasting time. It was found that:

The melting $(\text{NH}_4)_2\text{SO}_4$ and acidifying agents were decomposed slowly below 400 °C, promoting the leaching recoveries of REEs by generating large amounts of $\text{NH}_4\text{RE}(\text{SO}_4)_2 \cdot 4\text{H}_2\text{O}$. However, after temperatures exceeding 400 °C, $(\text{NH}_4)_2\text{SO}_4$ and the acidifying agents started to decompose rapidly. The generation of $\text{NH}_4\text{RE}(\text{SO}_4)_2 \cdot 4\text{H}_2\text{O}$ was cut down, due to the lack of molten $(\text{NH}_4)_2\text{SO}_4$ and the acidifying agents, leading to the drop in leaching recovery.

The acidity of the leaching solution was maintained with residual $(\text{NH}_4)_2\text{SO}_4$, preventing hydrolysis of $\text{RE}_2(\text{SO}_4)_3$ to form precipitates. If the roasting time was too long, $(\text{NH}_4)_2\text{SO}_4$ would be excessively consumed and decomposed, resulting in the loss of REEs.

The increase in mass ratio of $(\text{NH}_4)_2\text{SO}_4$ to magnetic separation tailings led to excessive NH_4^+ and SO_4^{2-} in the leaching solution. The REEs ions also tended to precipitate with extra NH_4^+ and SO_4^{2-} in form of $\text{NH}_4\text{RE}(\text{SO}_4)_2$, leading to the loss of REEs.

(3) The leaching recoveries of La, Ce, and Nd reached 83.12%, 76.64%, and 77.35%, respectively. The rest of the REEs were deposited in monazite (REPO_4), which was difficult to decompose during the roasting process.

Acknowledgments: Financial support to this project is provided by the National Natural Science Foundation of China (51274061) and the National Program on Key Basic Research Project of China (2012CBA01205).

Author Contributions: Yan Zhou, He Yang, and Xiang-xin Xue conceived and designed the study; Yan Zhou and Shuai Yuan performed the experiments; Yan Zhou analyzed the data; He Yang and Xiang-xin Xue contributed reagents/materials/analysis tools; Yan Zhou wrote the paper.

Conflicts of Interest: The authors declare no conflict of interest. The founding sponsors had no role in the design of the study; in the collection, analyses, or interpretation of data; in the writing of the manuscript, and in the decision to publish the results.

References

- Huang, X.W.; Li, H.W.; Wang, C.F.; Wang, G.Z.; Xue, X.X.; Zhang, G.C. Development Status and Research Progress in Rare Earth Industry in China. *Chin. J. Rare Metals* **2007**, *31*, 279–288.
- Huang, X.W.; Zhang, Y.; Li, H.W. Development Trend and Research Progress of Rare Earth Extraction in China. *Bull. Natl. Nat. Sci. Found. China* **2011**, *3*, 134–137.
- Cheng, J.Z.; Che, L.P. Current Mining Situation and Potential Development of Rare Earth in China. *Chin. Rare Earths* **2010**, *31*, 65–85.
- Yu, X.L.; Bai, L.; Wang, Q.C.; Liu, J.; Chi, M.Y.; Wang, Z.C. Recovery of Rare Earths, Niobium, and Thorium from the Tailings of Giant Bayan Obo Ore in China. *Metall. Mater. Trans. B* **2012**, *43*, 485–493. [[CrossRef](#)]
- Ding, Y.G.; Xue, Q.G.; Wang, G.; Wang, J.S. Recovery Behavior of Rare Earth from Bayan Obo Complex Iron Ore. *Metall. Mater. Trans. B* **2013**, *44*, 28–36. [[CrossRef](#)]
- Wang, L.; Zhong, B.; Liang, T.; Xing, B.; Zhu, Y. Atmospheric thorium pollution and inhalation exposure in the largest rare earth mining and smelting area in China. *Sci. Total Environ.* **2016**, *572*, 1–8. [[CrossRef](#)] [[PubMed](#)]
- Wang, L.; Liang, T. Accumulation and fractionation of rare earth elements in atmospheric particulates around a mine tailing in Baotou, China. *Atmos. Environ.* **2014**, *88*, 23–29. [[CrossRef](#)]
- Xu, G.X. *Rare Earths*, 2nd ed.; Metallurgical Industry Press: Beijing, China, 2012; Volume 1, pp. 364–468.
- Gupta, C.K.; Krishnamurthy, N. *Extractive Metallurgy of Rare Earths*; CRC Press: Boca Raton, FL, USA, 2005; pp. 28–56 and 133–158.
- Liu, X.W.; Feng, Y.L.; Li, H.R.; Yang, Z.C.; Cai, Z.L. Recovery of valuable metals from a low-grade nickel ore using an ammonium sulfate roasting-leaching process. *Int. J. Miner. Metall. Mater.* **2012**, *19*, 377–383. [[CrossRef](#)]
- Saleh, H.I.; Hassan, K.M. Extraction of zinc from blast-furnace dust using ammonium sulfate. *J. Chem. Technol. Biotechnol.* **2004**, *79*, 397–402. [[CrossRef](#)]
- Yang, H.; Rong, Y.; Han, C.; Tang, R.; Xue, X.X.; Li, Y.; Li, Y.N. Magnetizing roast and magnetic separation of iron in rare-earth tailings. *J. Cent. South Univ.* **2016**, *23*, 1899–1905. [[CrossRef](#)]

13. Singh Mudher, K.D.; Keskar, M.; Venugopal, V. Solid state reactions of CeO₂, ThO₂ and PuO₂ with ammonium sulphate. *J. Nucl. Mater.* **1999**, *265*, 146–153. [[CrossRef](#)]
14. Yu, Y.F.; Qi, C.Y. Magnetizing roasting mechanism and effective ore dressing process for oolitic hematite ore. *J. Wuhan Univ. Technol. Mater. Sci. Edit.* **2011**, *26*, 176–181. [[CrossRef](#)]
15. Bale, C.W.; Chartrand, P.; Degterov, S.A.; Eriksson, G.; Hack, K.; Ben Mahfoud, R.; Melançon, J.; Pelton, A.D.; Petersen, S. FactSage thermochemical software and databases. *Calphad* **2002**, *26*, 189–228. [[CrossRef](#)]
16. Kiyoura, R.; Urano, K. Mechanism, Kinetics, and Equilibrium of Thermal Decomposition of Ammonium Sulfate. *Ind. Eng. Chem. Proc. Des. Dev.* **1970**, *9*, 489–494. [[CrossRef](#)]
17. Jariwala, M.; Crawford, J.; LeCaptain, D.J. In Situ Raman Spectroscopic Analysis of the Regeneration of Ammonium Hydrogen Sulfate from Ammonium Sulfate. *Ind. Eng. Chem. Res.* **2007**, *46*, 4900–4905. [[CrossRef](#)]
18. Kosova, D.A.; Emelina, A.L.; Bykov, M.A. Phase transitions of some sulfur-containing ammonium salts. *Thermochim. Acta* **2014**, *595*, 61–66. [[CrossRef](#)]
19. Zhang, S.R.; Li, H.W.; Ma, X.F. Study on Decomposition of High Grade Bastnasite in Calcination. *J. Guangdong Non-Ferrous Metals* **1997**, *7*, 113–116.
20. Liu, K.W.; Chen, T.L. Studies on the thermal decomposition of ammonium sulfate. *Chem. Res. Appl.* **2002**, *14*, 737–738 and 765.
21. Fan, Y.Z.; Cao, F.H. Thermal Decomposition Kinetics of Ammonium Sulfate. *J. Chem. Eng. Chin. Univ.* **2011**, *25*, 341–346.



© 2017 by the authors. Licensee MDPI, Basel, Switzerland. This article is an open access article distributed under the terms and conditions of the Creative Commons Attribution (CC BY) license (<http://creativecommons.org/licenses/by/4.0/>).